# Three Wave Mixing as the Limit of Nonlinear Dynamics Theory for Nonlinear Transmission Line Type Metamaterials

Sameh Y. Elnaggar, *Member, IEEE,* and Gregory N. Milford, *Member, IEEE*

***Abstract*—Using nonlinear dynamics theory, a linear time periodic equivalent circuit of a sinusoidally pumped distributed transmission line type metamaterial is proposed. For small pump power and sufficient number of unit cells, it is shown that three wave mixing, coupled with phase matching, can be used to determine the frequencies of the autonomous components and their propagation behaviour. The resulting signal and idler waves satisfy the well-known Manley-Rowe relation. However, unlike nonlinear dynamics theory and stability analysis, three wave mixing can be inaccurate for relatively large input power levels and/or short transmission lines. In particular, the waveform profile and consequently radiation of the autonomous frequencies located inside the light cone cannot be described using three wave mixing and nonlinear dynamics and/or stability analysis must be applied.**

***Index Terms*—Nonlinear Metamaterials, Nonlinear Dynamics, Composite Right Left Handed Transmission Lines**

## I. Introduction

Metamaterial structures constructed with nonlinear unit cell components have demonstrated a range of interesting behaviours, such as harmonic generation and amplification [1], [2], parametric frequency leaky wave radiation [3] and multiple parametric frequency generation [4]. Such structures offer a potential technology that both complements existing transistor technologies, and extends the range to terahertz and optical frequencies for signal processing applications [5]. Still lacking though are design procedures based on a rigorous understanding of the interactions between forward and backward propagating waves in the presence of the strong and controlled distributed nonlinearities.

Accurate analysis of nonlinear distributed structures can be quite challenging. Inspired by nonlinear optics approaches [6], Nonlinear Composite Right-Left Handed Transmission Lines (NL CRLH TL) have been analysed in terms of the interaction of autonomous parametric waves excited by the coupling of a strong input pump signal and its higher harmonics with the nonlinearity [7]. This frequency domain approach, referred to as three wave mixing (TWM), assumes stable steady state behaviour and matching of wave numbers and frequencies of only three significant terms, namely the pump, signal and idler (parametric) waves. However the tendency for NL CRLH TL structures to exhibit instability [8] and the excitation of multiple incommensurate autonomous frequencies [4] can render *wave mixing* approaches impractical due to the necessity of knowing such complex behaviour a priori. Another more fundamental concern is that TWM assumes a weak nonlinearity, which although satisfactory for optical media illuminated by high intensity lasers (eg. Kerr nonlinearity [6]), may not be valid when applied to finite length metamaterial structures with significantly higher order nonlinearities (eg. varactor diodes [9]).

Traditionally nonlinear systems are described in the time domain, usually with the problem cast in the form of a set of first order differential equations (state space formalism) that accurately reflect the underlying physics, with amplitude nonlinearities and variable time delay effects (frequency dispersion) automatically included [10].

S.Y.E and G.N.M are with the School of Engineering and Information Technology, University of New South Wales, Canberra, emails: s.elnaggar@unsw.edu.au, g.milford@adfa.edu.au

To rigorously describe TL type metamaterials excited by a continuous sinusoidal (pump) input, a framework based on nonlinear dynamics (NLD) theory was developed in [11], [12]. Using this approach, the autonomous frequencies and their spatial distribution were calculated using the time periodic (or *T-periodic*) system, resulting from linearization at a limit cycle. It was shown that the spontaneous generation of the autonomous components is equivalent to a bifurcation of the limit cycle to a more complex limit set: an *n-dimensional* torus [11]. Importantly, good agreement between time domain numerical predictions and measurements has been demonstrated, including the autonomous frequency values in the vicinity of the lowest Bragg frequency [13]. In this case, the effective homogeneity condition is violated and the TL behaves more like a photonic crystal [14]. Additionally, NLD predicts that, whenever bifurcation occurs, there is potentially an infinite number of generated autonomous components; they are nothing but the time harmonics due to the time periodicity of the linearized system.

In contrast to a NLD analysis, the application of a simpler TWM analysis to a NL CRLH TL structures is more appealing. Given the choice, it is desirable to have some criteria to guide this decision. In this article we show that TWM is the limit of NLD when the nonlinearity is small and the distributed structure extends to infinity. Section II briefly reviews the NLD analysis of a NL CRLH TL structure. Modeling perturbations to the steady state limit cycle allows determination of the autonomous frequencies and their waveforms, including the onset of bifurcation and/or instability. In Section III we describe a *T-periodic* unit cell equivalent circuit, which for small pump amplitudes describes perturbations about the limit cycle. Then in Section IV, assuming the only significant spectral components are the pump, signal and idler, the TWM phase matching condition is derived for the NL CRLH structure. Finally, Section V demonstrates the relative performance of TWM based analysis compared to NLD results for determining the magnitude and phase of the spontaneously generated autonomous waves components, for a range of pump amplitudes and frequencies.

## II. Non-Linear Dynamics

In this section, we briefly review how NLD theory is applied to study the properties of NL CRLH TL structures (for a more detailed analysis please see [12]). The first step is to describe the system using a nonlinear state space model (SSM) [10], [15]

$$\dot{\mathbf{x}}(t) = f\left(\mathbf{x}(t), \mathbf{u}(t)\right), \tag{1}$$

where $\mathbf{x}$ and $\mathbf{u}$ are the state and excitation vectors, and $f$ is some nonlinear operator [15], [16]. For the case of excitation by a single sinusoidal (pump) input at frequency $f_P$, the dynamics of the bifurcation can be investigated by linearising the response at the limit cycle. As was previously shown, the linearized system is *T-periodic*, where $T = 1/f_P$. Consider the application of NLD theory to the NL CRLH TL structure shown in Fig. 1, which consists of a cascade of identical unit cells of series and shunt lumped elements. Resistors $R$ in each unit cell account for any conductor or parasitic Ohmic losses in the structure. Fig. 2 shows the dispersion relation extracted from

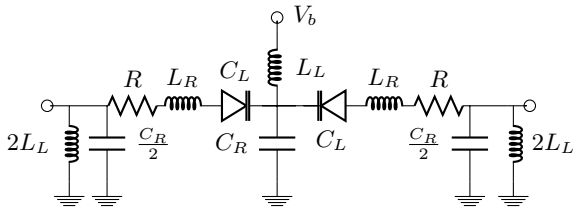


Fig. 1. A lumped circuit model of two unit cells of a N-stage NL CRLH TL. Nonlinearity is implemented with varactors having voltage dependent capacitance $C_L$. Typical values: $R = 0.5\ \Omega$, $L_L = 1.797$ nH, $C_R = 1.100$ pF, $L_R = 2.700$ nH, $C_L = C_{L0} = 0.730$ pF at bias voltage $V_b$=+1.290 V for a balanced configuration [17].

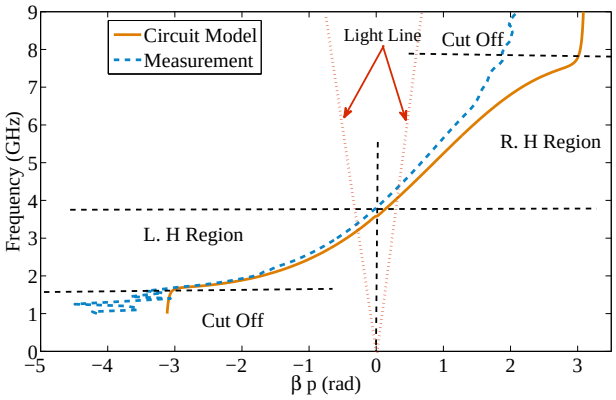


Fig. 2. The dispersion characteristics of the LTI system using the lumped circuit model and compared to the characteristics extracted from measurements.The light lines and different regions are highlighted. The light lines intersect the dispersion characteristics at $f \approx 3.2$ GHz and $f \approx 4.2$ GHz. The transition frequency ($\beta p = 0$) is 3.6 GHz.

measurements [17], compared to the dispersion response computed using the lumped circuit model in Fig. 1, where the varactors were replaced by $C_{L0}$, the capacitance determined by the bias voltage $V_b$. Since all other circuit components are constants, this model is denoted here as linear time invariant (LTI). Between the light lines shown in Fig. 2, the NL CRLH TL acts as a leaky wave antenna [3], [14]. In Section V, we discuss the influence of the nonlinearity on the direction of the main beam when the autonomous frequencies are inside the light cone.

To construct the state vector $\mathbf{x}$ in (1), $N_s$ independent inductor currents and capacitor voltages are chosen as the state variables. For a given input pump amplitude we numerically solve (1) to find the states at discrete time steps. Whenever the input is below some threshold, the system reaches a limit cycle. However, increasing the input power above the threshold renders the limit cycle unstable, resulting in the emergence of autonomous frequency components that propagate along the TL. In this context, the onset at which the input excites autonomous components identifies a bifurcation condition.

We now consider a small disturbance or perturbation vector $x(t)$ to The disturbance $x(t)$ at the limit cycle solution $\bar{\mathbf{x}}(t)$. $x(t)$ can be described using a *T-periodic* system of first order differential equations.

$$\dot{x} = \left.\frac{\partial f}{\partial \mathbf{x}}\right|_{\bar{\mathbf{x}}} x \;=\; \mathbf{J}(\mathbf{x},t)|_{\bar{\mathbf{x}}}\; x \tag{2}$$

$\mathbf{J}$ is the $N_s$ x $N_s$ Jacobian matrix evaluated at the limit cycle; hence is *T-periodic*. Generally, the solution of (2) is not necessarily periodic and, for any initial disturbance $x(t_o)$ at time $t_o$, can be written as [18]

$$x(t) = \tilde{\mathbf{P}}(t)\, e^{(t-t_o)\tilde{\mathbf{R}}}\, \mathbf{S}^{-1}\, x(t_o), \tag{3}$$

where $\tilde{\mathbf{P}}(t)$ is a *T-periodic* matrix and $\tilde{\mathbf{R}}$ is a diagonal matrix; its diagonal elements $\mu_i \equiv \sigma_i + j\theta_i/T$ are the Floquet exponents. $\mathbf{S}$ is a constant valued similarity transform matrix that ensures matrix $\tilde{\mathbf{R}}$ has diagonal form (see [12] for details). Noting that $\mathbf{S}$ and $x(t_o)$ are constants, we observe that all of the time dependent behaviour is described by the product of the $\tilde{\mathbf{P}}(t)$ and exponential matrices, which has time varying column vectors of the form:

$$\eta_i(t) = e^{\mu_i(t-t_o)}\tilde{\mathbf{p}}_i(t) \;+\; cc, \tag{4}$$

where $\tilde{\mathbf{p}}_i(t)$ is the $i^{\text{th}}$ column of $\tilde{\mathbf{P}}(t)$. If $\sigma_i > 0$, the $\eta_i$ solution grows with time and hence identifies an instability condition. At the onset of bifurcation, typically only one or a few $\sigma_i \approx 0$ and the remaining $\sigma_i$ values are negative. Hence these $\mu_i$ terms dominate the solution as time increases. This affords us a means to synthesise a disturbance $x(t)$ that has the same stability characteristics as (3) with arbitrary initial states $x(t_o)$. We identify the dominant Floquet exponents, retain only these terms in the $\tilde{\mathbf{P}}(t)$ and $\tilde{\mathbf{R}}$ matrices while zeroing out the rest, and compute $x(t)$ from (3) using the modified $\tilde{\mathbf{P}}(t)$ and $\tilde{\mathbf{R}}$. In the subsequent discussion this will be referred to as the *Stability* method. Observation of the spectra for the time series $\mathbf{x}(t)$ satisfying (1) typically shows multiple spectral lines, corresponding to radian frequencies $\omega = |\theta_i \pm 2k\pi|/T, k = 1, 2\ldots$. In this way the Floquet exponents determine both the amplitude (stability) and frequency of states $x(t)$. The imaginary part $\theta_i$ of $\mu_i$ determines the autonomous frequencies.

## III. $T$-Periodic Equivalent Circuit

Since all of the states in $x(t)$ are either voltages or currents, an equivalent circuit model for the disturbance $x(t)$ can be developed by identifying the $i, v$ relationships between elements in a given row of $\mathbf{J}$ and that row's voltage/current variable in $x(t)$. The result for a single unit cell is shown in Fig. 3.

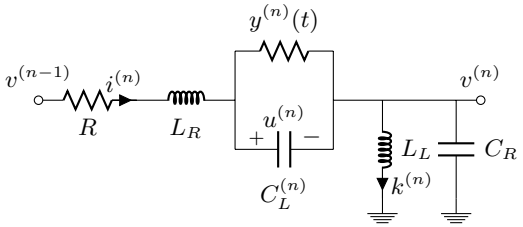


Fig. 3. Equivalent Circuit of the $n^{\text{th}}$ unit cell of the $T$-Periodic system.

Furthermore, by considering small pump voltage amplitudes, the dependence of the nonlinear varactor capacitance $C_L$ and admittance $y$ on the time varying voltage $u(t)$ can be linearised about the bias voltage. In a manner similar to the development of linear circuit models for active devices such as transistors and diodes, $\mathbf{J}$ can be represented by an equivalent circuit model. Fig. 3 shows the equivalent circuit of one unit cell representing the set of linearized equations of the TL given in Fig. 1. Provided $u(t)$ is dominated by the pump, ie. $u(t) = u_P(t)$, the series capacitance $C_L^{(n)}$ at the $n^{\text{th}}$ stage is *T-periodic* and is given by

$$C_L^{(n)}\left(u_P^{(n)}\right) = C_{L0} + \left[\frac{\partial C_L}{\partial u}\right]_{V_b} u_P^{(n)}(t) = C_{L0}\left(1 + M_0^{(n)} u_P^{(n)}(t)\right), \tag{5}$$

where $u_P^{(n)}$ is the voltage across $C_L^{(n)}$ determined by the pump wave and its higher harmonics, $M_0^{(n)} \equiv (-1)^{n+1}/(\psi_0 + V_B)$ and $\psi_0$ depends on the varactor model [12]. Similarly, the *T-periodic* admittance $y^{(n)}(t)$ is given by

$$y^{(n)}(t) = M_0^{(n)}\left(1 + M_0^{(n)} u_P^{(n)}(t)\right) i_P^{(n)}(t), \tag{6}$$

where $i_P^{(n)}(t)$ is the current due to the pump and its higher harmonics.

Note that (5) and (6) are essentially the first two terms in a Taylor series expansion of the varactor's capacitance and admittance dependence on pump voltage $u_P^{(n)}$ about the bias point $V_b$, where the higher order terms can be neglected provided the pump amplitude $u_P^{(n)} \ll \psi_0 + V_b$.

In general, the strength of the nonlinearity increases as the slope of the C-V at the bias voltage and the magnitude of the pump voltage increase (refer to Eq. 5). Thus, it is expected that nonlinearity can be considerably higher for abrupt C-V devices. For the varactors shown in Fig. 1, $\psi_o = 2.06$V and $V_b = 1.290$V hence the nonlinear term can be approximated to $0.3C_{L0}u_P^{(n)}$. The nonlinearity factor

$$M \equiv \frac{1}{C_{L0}}\left|\frac{\partial C}{\partial u}\right|_{V_b}|u_P| = \frac{|u_P|}{\psi_0 + V_b} \approx 0.3|u_P|. \tag{7}$$

Although the pump and its higher harmonics are periodic, the circuit is not periodic in the spatial domain. This is evident by noting that the dispersive behaviour of CRLH TLs implies that the pump and its higher harmonics do not propagate with the same speed. Due to the back-to-back varactors configuration, the effect of the nonlinearity is sub-wavelength (microscopic) which is emphasized by the $(-1)^{n+1}$ term in $M_0^{(n)}$ in Eqs. (5) and (6). This means that, generally, the *finite size* of the unit cell plays an essential role in describing the propagation of the autonomous waves, as was experimentally and numerically observed [13], [19].

Before embarking on the details of the TWM analysis, it is helpful to highlight the main differences between the *T-periodic* equivalent circuit in Fig. 3 and the nonlinear equivalent circuit in Fig. 1. The circuit in Fig. 3 represents the time periodic equivalent circuit of the circuit in Fig. 1. The solution of (1) for the circuit in Fig. 1 can be readily determined by a brute-force ODE solver, and completely determines the current and voltage values as a function of time. However, valuable insight into the interaction of propagating waves and circuit quantities is lost. On the other hand, the linearized circuit encapsulates the effect of the pump wave in the *T- periodic* lumped parameters and hence presents the problem in a cause and effect-like form. This is identical to traditional analysis of transistors and amplifiers. However the analysis here is linearized around a limit cycle rather than at a bias point [12].

## IV. Three Wave Mixing

In this Section we apply a TWM approach to the structure of Fig. 1, where we assume that the pump excitation excites only two other propagating waves in the NL CRLH structure, namely the Idler (I) and the Signal (S) (not to be confused with the matrix $\mathbf{S}$ in (3), which will not be referred to in the subsequent discussion), such that

$$\omega_P = \omega_S + \omega_I. \tag{8}$$

This approach is common practice in nonlinear optics where the homogeneous optical media typically exhibit very weak nonlinearities [6]. Any state variable $x$ (for example $i^{(n)}$ or $v^{(n)}$) can be written as

$$x(t) = x_S(t) + x_I(t) + cc. \tag{9}$$

Generally speaking, the pump current $i_P^{(n)}$ is periodic with frequency $f_P$ and hence can be expanded in a Fourier series. Assuming that the *nonlinearity is weak*, usually the case for small input pump power, and noting that there is no DC component, $i_P^{(n)}$ can be simplified to

$$i_P^{(n)} = I_1 \cos(2\pi f_P t + \phi_1). \tag{10}$$

Similar expressions can be found for the other state variables. The equivalent circuit in Fig. 3 together with (5) and (6) allow us to write the following equations for the voltages and currents at the signal frequency $\omega_S$:

$$j\omega_S i_S^{(n)} L_R = v_S^{(n-1)} - i_S^{(n)} R - v_S^{(n)} - u_S^{(n)}, \tag{11}$$

$$j\omega_S k_S^{(n)} L_L = v_S^{(n)}, \tag{12}$$

$$j\omega_S v_S^{(n)} C_R = i_S^{(n)} - k_S^{(n)} - i_S^{(n+1)} \text{ and} \tag{13}$$

$$i_S^{(n)} = M_0^{(n)} \frac{\omega_S}{\omega_P} i_P^{(n)} \bar{u}_I^{(n)} + j\omega_S C_{L0} u_S^{(n)}. \tag{14}$$

In the last equation, the voltage $u^{(n)}$ was expanded in the signal and (conjugate) idler components as given by (9); the *T-periodic* $C_L$ and $y$ couple the signal with the complex conjugate of the idler. Equations for the idler can be readily obtained from the above ones by exchanging $S$ and $I$. In the absence of the pump wave ($i_P^{(n)} = 0$), (11) - (14) describe a LTI CRLH TL.

It is worth noting that no condition was imposed on the spatial distribution of the signal and idler. However if one seeks wave solutions, Bloch-Floquet theory can be applied to an infinite length CRLH structure [14] to express the generic state variable $x_\Pi$, for $\Pi = S, I$, in the form $x_\Pi^{(n)} = x_\Pi^{(n-1)} e^{-j\beta_\Pi p}$, where $p$ is the length of the unit cell. Substituting back the assumed form in (14), shows that the coupling between the signal and idler can be maximized when

$$(\beta_P - \beta_S - \beta_I)\, p \pm \pi = 2m\pi,\ m = 0, \pm 1, \pm 2, \cdots, \tag{15}$$

which is essentially the phase matching condition. The $\pm\pi$ term is due to the back to back connection of the varactors, which is equivalent to *material polling* in nonlinear optical media. However in the current situation, it is microscopic in nature. Together (8) and (15) along with the dispersion characteristic identify $\omega_S$ and $\omega_I$ for a given pump frequency $\omega_P$.

The *T-periodic* equivalent circuit and the set of (11) - (14) guarantee that the signal and idler satisfy the well-known Manley-Rowe equations. This can be shown by noting that the power $P_\Pi^{(n)}$ generated due to the nonlinearity is given by $P_\Pi^{(n)} = 1/2Re\left(u_\Pi^{(n)} \bar{i}_\Pi^{(n)}\right)$, which can be expanded using (11) and (14) to give

$$P_S/\omega_S = P_I/\omega_I, \tag{16}$$

that is, the Manley-Rowe relation.

## V. Results and Discussion

The system of equations (11) - (14) describes the local interaction between the signal and idler waves as they propagate along the TL. For practical scenarios, the TL is finite. Here, we will consider $N$ stages only with $6N$ unknowns: $v_S^{(n-1)}, i_S^{(n)}, u_S^{(n)}, v_I^{(n-1)}, i_I^{(n)}$ and $u_I^{(n)}$, $n = 1, 2, \ldots N$. Note that $k_{S,I}^{(n)}$ are readily obtained from $v_{S,I}^{(n)}$ via (12). Given the boundary currents and voltages $i_S^{(N+1)}, i_I^{(N+1)}, v_S^{(N)}$, and $v_I^{(N)}$; and the spatially varying pump current $i_P^{(n)}$, (11) - (14) form a set of inhomogeneous linear algebraic equations, which can be simultaneously solved to determine all currents and voltages.

To obtain solutions which match with results obtained from the nonlinear system (1), the boundary currents and voltages are determined from the spectra of the time series solution $\mathbf{x}(t)$ in (1) at $\omega_S$ and $\omega_I$ for any given $\omega_P$.

In addition the Stability analysis described in Section II is invoked to compute the signal and idler amplitude and phase values calculated from the time series vector $x(t)$ in (3). Figs. 4 and 5 show two typical results, for $N = 20$. From Fig. 4 it is evident that TWM accurately predicts the signal and idler magnitudes and phases.. In this case $f_P = 4.5$ GHz and the onset of bifurcation occurs at $V_{P0} = 0.39$ V,

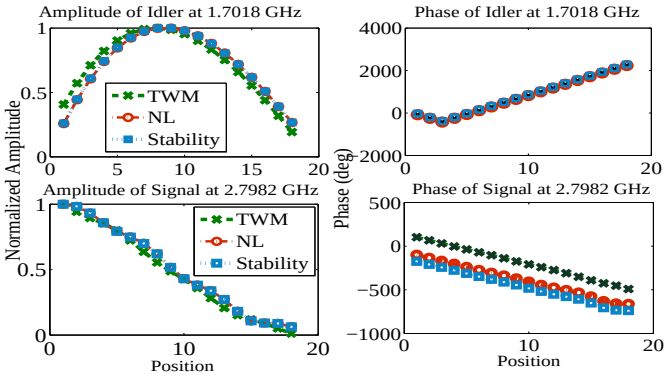


Fig. 4. Normalised amplitude and phase of the autonomous frequencies calculated for $f_P = 4.5$ GHz, $V_P = V_{P0} = 0.39$ V, and $N = 20$ TWM (green traces): solution of (11) to (14) for selected $n$; NLD (red traces): spectral values from time series solution $\mathbf{x}(t)$ in (1); Stability (blue races): spectral values from time series solution $x(t)$ in (3).

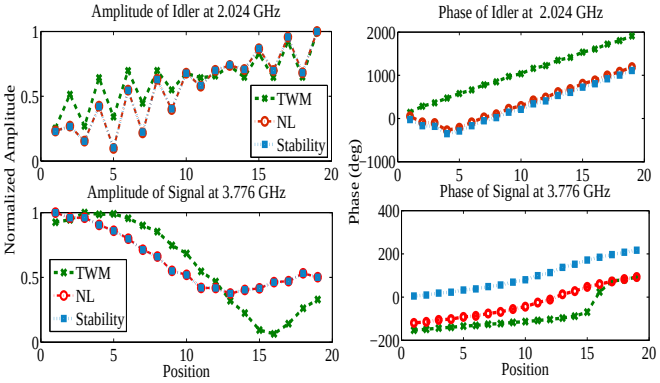


Fig. 5. As for Fig. 4 but with $f_P = 5.8$ GHz, $V_P = 1.4$ V and $N = 20$.

where $V_{P0}$ is the applied pump voltage. However when $f_P$ increases to 5.8 GHz, the onset of bifurcation increases to 1.4 V where this larger pump voltage excites a stronger nonlinear response.

In passing, it is useful to point out to the rationale behind using the two frequencies $f_P = 4.5$ GHz, and $f_P = 5.8$ GHz as the two test cases. In the vicinity of 4.5 GHz, it was numerically and experimentally found that the onset of bifurcation is obtained with a minimum pump amplitude (Ref. [12], Fig. 3). Therefore at 4.5 GHz the smaller pump amplitude implies a relatively weak nonlinearity. However above around 5.5 GHz, the onset of bifurcation appears at larger pump amplitudes, implying a relatively stronger nonlinearity. When $f_P$= 6 GHz the nonlineariy becomes significantly high such that the varactor nonlinear model is questionable. So as a compromise we used 5.8 GHz.

As Fig. 5 illustrates, the disparity between the TWM and the NLD and Stability analysis results suggests the TWM method is less accurate at this higher pump level. The disagreement between NLD and stability analysis on one hand and TWM on the other can be explained by examining the underlying assumptions. When the nonlinearity is weak, it is reasonable to assume that only the pump wave mediates the interaction between the time harmonics (i.e, ignoring the effect of second and higher harmonics). In general though this is not the case. Additionally, TWM limits the analysis to the pump plus two dominant time harmonics (signal and idler). However, according to Bloch-Floquet theorem the time periodicity of the system dictates that a complete solution will be the linear combination of all time harmonics ($f + mf_p, m \in \mathbb{Z}$). In contrast, the Stability approach encapsulates the pump and all its higher harmonics in the limit cycle, hence all time harmonics emerge naturally in the stability analysis as a result of the ambiguity of the phase of the Floquet multipliers [12]. So when $f_P$ changes from 4.5 to 5.8 GHz, the onset of bifurcation increases from a pump amplitude of 0.39 V to 1.4 V, which increases the nonlinearity. This in turn renders TWM questionable, which is indeed why TWM did not predict the correct amplitudes as shown in Fig. 5. Interestingly Fig. 5 indicates the phase shift is still accurate over many unit cells; this corresponds to an accurate phase shift per unit cell and, consequently, accurate phase velocity. It is worth noting that the Stability analysis of (3) predicts the phase profile within a constant phase factor; this is due to the fact that $\eta_i$ in (4) represents a solution that can be multiplied by an arbitrary complex number (ie. phase offset). So not only does a large $V_{P0}$ render the TWM approximation questionable, it also modulates the TL characteristic impedance and hence allows multiple reflections from the input and output ports; and between the unit cells. On the other hand, the NLD and Stability analysis methods stem from the local interactions of the state variables (mesh and nodal analysis); any variations due to the pump and its higher harmonics are encapsulated in the limit cycle around which the linearized solution revolves.

From (5) and (7), it is clear that the strength of the nonlinearity for $f_P = 5.8$ GHz is 3.5 times its value at $f_P = 4.5$ GHz. In the general case, it is difficult to put a single number that separates between the weak and strong nonlinearity regimes. This is because for a general distributed system, the effect of the nonlinearity is accumulative depending on the phase of autonomous components as well as terminations and the exact circuit configuration. In the case in hand, however, an estimate value of $|M| = 0.1$ can be used to separate the two regimes. This value is midway between the values that $|M|$ attains at $f_P = 4.5$ GHz ($\approx 0.06$), and $f_P = 5.8$ GHz ($\approx 0.2$).

The autonomous component at frequency 3.776 GHz lies inside the light cone and hence radiates. It is found via numerical analysis that TWM cannot predict the waveform and phase for other components inside the light cone. This means that NLD and/or Stability analysis must be used to determine the radiation properties. Fig. 6 shows the waveform and phase of another two autonomous frequencies inside the light cone emphasizing the need to use NLD and Stability analysis. It is worth noting that the phase velocity is co-directional with the pump (negative slope of phase, Fig. 6, $f_P = 5.0$ GHz) when the autonomous frequency is below the transition frequency ($f \approx 3.6$ GHz). However, increasing the pump frequency will eventually results in an autonomous frequency that is in the RH regime. Such frequency has a phase velocity that is contra-directive with the pump (indicated by the positive slope of the phase in Fig. 6, $f_P$= 5.6 GHz). Due to the spatial variation of the amplitude (Figs. 5 and 6), the exact radiation pattern depends on the exact amplitude and phase profile of the current on the NL CRLH TL.

If the number of stages $N$ is increased from 20 to 80, the autonomous components appear at a lower $V_{P0}$ of 0.505 V. Fig. 7 shows the calculated amplitude and phase of the autonomous components. It is evident that the TWM accuracy has significantly increased (compared to Fig. 5). This is partly due to the lower $V_{P0}$ and the larger number of unit cells.

Finally, the phase matching condition (15) is numerically verified. First, the phase mismatch $\Delta\beta$ is defined as

$$\Delta\beta p \equiv |\beta_P - \beta_S - \beta_I|\, p, \tag{17}$$

which is equal to $(2m+1)\pi$ whenever the phase matching condition (15) holds. In particular, $\Delta\beta p = \pi$ for $m = 0$. Second, the phase shift $\beta_S$, $\beta_I$ and $\beta_P$ are determined from the LTI dispersion relation

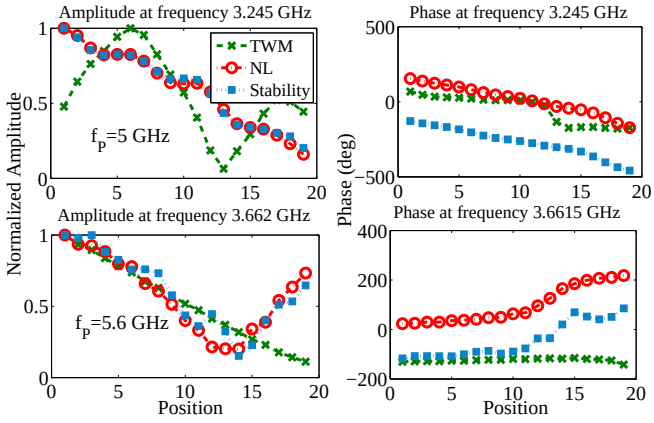


Fig. 6. Normalized voltage and phase of two autonomous frequencies inside the light cone. Left: $f_P = 5.0$ GHz, Right: $f_P = 5.6$ GHz

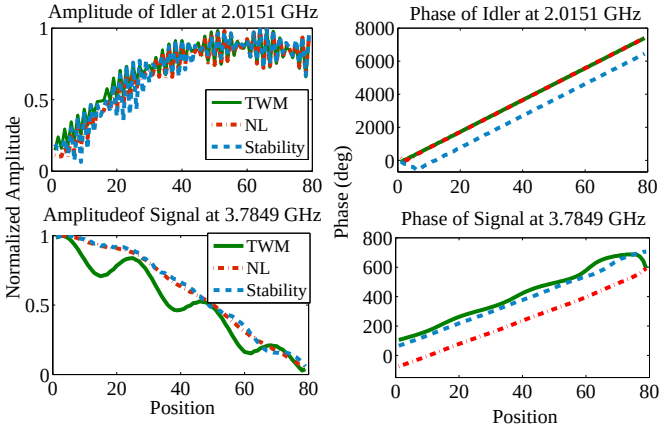


Fig. 7. As for Fig. 4 but with $f_P = 5.8$ GHz, $V_P = 0.505$ V and $N = 80$.

depicted in Fig. 2 and from the phases of the autonomous components such as the ones depicted in Figs. 4, 5 and 7 by fitting the phase response to a straight line and calculating its slope. Then the phase mismatch $\Delta\beta p$ is calculated using (17) and presented in Fig. 8. It is clear that the phase matching condition holds within an error bound of less than 10%. The discrepancy between LTI and NLD results is attributed to the *slight* change of the phase shift due to the presence of the pump. Interestingly, the directions of propagation of the autonomous components change as function of the pump frequency $f_P$. Below $f_P = 4.5$ GHz (region A), both the signal and idler phase velocities are co-directional with the pump phase velocity. Because they are in the left hand band, the energy (or equivalently, the group velocity) propagates in the backward direction toward the source. For the phase matching condition (15) to hold as pump frequency increases, the idler direction switches in region B and subsequently, the direction of the signal changes in region C. This behaviour was previously described based on a purely numerical approach [19].

As long as the spatial variation of the autonomous frequency is slow, the direction of the radiated main beam can be determined by the phase alone. In this case, the main beam changes from the backward end fire to broadside and then toward the forward end fire. However, when the nonlinearity increases the amplitude variation smears out the radiation pattern equivalent to the effects of amplitude tapering in an aperture antenna. For the NL CRLH TL modeled by the lumped circuit in Fig. 1, the onset of bifurcation $V_{P0}$ attains a local

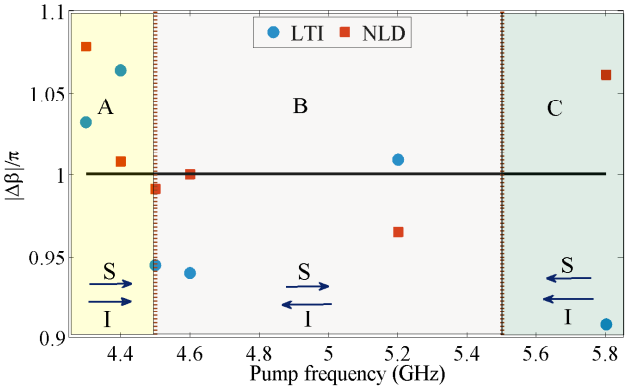


Fig. 8. Phase mismatch $|\Delta\beta/\pi|$ (17) with $\beta$ values from Fig. 2, compared to values calculated from the phases of the respective spectral components of the time series solution $\mathbf{x}(t)$ in (1). $f_P = 4.4 - 5.8$ GHz and $N = 20$

minimum close to the transition frequency. $V_{P0}$ and consequently the nonlinearity factor $M$ double at the right hand edge of the light cone, resulting in an increased amplitude for the *T-periodic* circuit elements depicted in Fig. 3 and described by (5) and (6). The phase change at the right edge coupled with the strong nonlinearity, increase the spatial variation between two consecutive unit cells of the lumped elements given by (5) and (6). This has the effect of enhancing the local interaction with the autonomous components, resulting in a *smeared* radiation pattern, as was experimentally observed from measuring the radiation pattern of the NLCRLH TL [3].

## VI. Conclusion

We exploited the nonlinear dynamics theory to derive the three wave mixing method and carefully examined the underlining assumptions for a distributed transmission line type metamaterial. Using the system Jacobian, a time periodic equivalent circuit was proposed and analyzed to determine the propagation properties of the autonomous components. Through detailed numerical simulations, it was demonstrated that three wave mixing is capable of providing accurate magnitude and phase profiles throughout the structure, particularly for small pump power and long transmission lines. The phase matching condition was derived and found to agree with previous measurements and numerical results. However, for strong nonlinearities due to a strong pump or a short TL, where multiple reflections are expected, nonlinear dynamics theory provides a more rigorous and reliable framework compared to TWM to study the autonomous components.

## References

[1] A. B. Kozyrev, H. Kim, A. Karbassi, and D. W. van der Weide, "Wave propagation in a nonlinear left-handed transmission line media," *Appl. Phys. Lettr.*, vol. 87, no. 121109, 2005.
[2] G. N. Milford and G. V. Eleftheriades, "2d multiplier with left-handed focusing lens for terahertz signal generation," in *2013 IEEE Antennas and Propagation Society International Symposium (APSURSI)*, July 2013, pp. 1182–1183.
[3] G. N. Milford and M. J. Gibbons, "Parametric frequency radiation from a nonlinear crlh transmission line," in *Microwave Conference Proceedings (APMC), 2011 Asia-Pacific*. IEEE, 2011, pp. 538–541.
[4] L. Chen and G. N. Milford, "Parametric signal behaviour in a nonlinear left-handed transmission line," *IEEE Antennas and Propagation Society International Symposium (APSURSI)*, 2012.
[5] M. Lapine, I. V. Shadrivov, and Y. S. Kivshar, "*Colloquium* : Nonlinear metamaterials," *Rev. Mod. Phys.*, vol. 86, pp. 1093–1123, Sep 2014.
[6] R. W. Boyd, *Nonlinear optics*, 3rd ed. Boston: Academic Press, 2008.
[7] A. B. Kozyrev and D. W. van der Weide, "Nonlinear left-handed transmission line metamaterials," *Journal of Physics D: Applied Physics*, vol. 41, no. 17, p. 173001, 2008.

[8] D. A. Powell, I. V. Shadrivov, and Y. S. Kivshar, "Multistability in nonlinear left-handed transmission lines," *Applied Physics Letters*, vol. 92, no. 26, 2008.
[9] A. B. Kozyrev and D. W. van der Weide, "Nonlinear wave propagation phenomena in left-handed transmission-line media," *IEEE Trans Microwave Theory and Tech*, pp. 238–245, January 2012.
[10] H. H. Khalil, *Nonlinear Systems*. Pearson Hall, 2002.
[11] S. Y. Elnaggar and G. N. Milford, "Stability analysis of nonlinear left handed transmission lines using floquet multipliers and bifurcation theory," in *IEEE International Symposium on Antennas and Propagation/USNC-URSI*, Fajardo, Puerto Rico, Jun. 2016.
[12] S. Elnaggar and G. Milford, "Description and stability analysis of nonlinear transmission line type metamaterials using nonlinear dynamics theory," *Journal of Applied Physics*, vol. 121, no. 12, 2017.
[13] S. Y. Elnaggar and G. N. Milford, "Analysis of nonlinear Left-Handed transmission lines using state space modelling," in *2015 International Symposium on Antennas and Propagation (ISAP) (ISAP2015)*, Hobart, Australia, Nov. 2015.
[14] C. Caloz and T. Itoh, *Electromagnetic Metamaterials Transmission Line Theory and Microwave Applications*, ser. Electromagnetic Metamaterials: Transmission Line Theory and Microwave Applications. Hoboken : Wiley, 2005.
[15] S. H. Strogatz, *Nonlinear dynamics and chaos: with applications to physics, biology, chemistry, and engineering*. Westview press, 2014.
[16] A. Suárez and R. Quéré, *Stability analysis of nonlinear microwave circuits*. Artech House, 2002.
[17] M. J. Gibbons and G. N. Milford, "Augmented harmonic balance stability analysis of nonlinear composite right-left handed transmission lines," in *Microwave Symposium Digest (MTT), 2011 IEEE MTT-S International*, June 2011, pp. 1–4.
[18] R. K. Miller and A. N. Michel, *Ordinary Differential Equations*. Academic Press, 1982.
[19] S. Y. Elnaggar and G. N. Milford, "Experimental and numerical analysis of nonlinear left handed transmission lines using three wave mixing," in *2nd Australian Microwave Symposium (AMS2016)*, Adelaide, Australia, Feb. 2016.